



THE UNIVERSITY *of* EDINBURGH

## Edinburgh Research Explorer

# Raman spectroscopy predicts the link between claw keratin and bone collagen structure in a mouse model of oestrogen deficiency

### Citation for published version:

Clare Caraher, M, Sophocleous, A, Renwick Beattie, J, O'Driscoll, O, Cummins, NM, Brennan, O, O'Brien, FJ, Ralston, SH, Bell, SEJ, Towler, M & Idris, AI 2017, 'Raman spectroscopy predicts the link between claw keratin and bone collagen structure in a mouse model of oestrogen deficiency', *BBA - Bioenergetics*.  
<https://doi.org/10.1016/j.bbadis.2017.10.020>

### Digital Object Identifier (DOI):

[10.1016/j.bbadis.2017.10.020](https://doi.org/10.1016/j.bbadis.2017.10.020)

### Link:

[Link to publication record in Edinburgh Research Explorer](#)

### Document Version:

Peer reviewed version

### Published In:

BBA - Bioenergetics

### General rights

Copyright for the publications made accessible via the Edinburgh Research Explorer is retained by the author(s) and / or other copyright owners and it is a condition of accessing these publications that users recognise and abide by the legal requirements associated with these rights.

### Take down policy

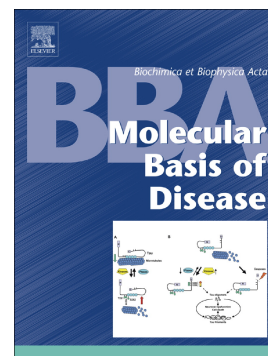
The University of Edinburgh has made every reasonable effort to ensure that Edinburgh Research Explorer content complies with UK legislation. If you believe that the public display of this file breaches copyright please contact [openaccess@ed.ac.uk](mailto:openaccess@ed.ac.uk) providing details, and we will remove access to the work immediately and investigate your claim.



## Accepted Manuscript

Raman spectroscopy predicts the link between claw keratin and bone collagen structure in a mouse model of oestrogen deficiency

M. Clare Caraher, Antonia Sophocleous, J. Renwick Beattie, Olive O'Driscoll, Niamh M. Cummins, Orlaith Brennan, Fergal J. O'Brien, Stuart H. Ralston, Steven E.J. Bell, Mark Towler, Aymen I. Idris



PII: S0925-4439(17)30384-8  
DOI: doi:[10.1016/j.bbadis.2017.10.020](https://doi.org/10.1016/j.bbadis.2017.10.020)  
Reference: BBADIS 64932

To appear in:

Received date: 26 July 2017  
Revised date: 21 September 2017  
Accepted date: 16 October 2017

Please cite this article as: M. Clare Caraher, Antonia Sophocleous, J. Renwick Beattie, Olive O'Driscoll, Niamh M. Cummins, Orlaith Brennan, Fergal J. O'Brien, Stuart H. Ralston, Steven E.J. Bell, Mark Towler, Aymen I. Idris , Raman spectroscopy predicts the link between claw keratin and bone collagen structure in a mouse model of oestrogen deficiency. The address for the corresponding author was captured as affiliation for all authors. Please check if appropriate. Bbadis(2017), doi:[10.1016/j.bbadis.2017.10.020](https://doi.org/10.1016/j.bbadis.2017.10.020)

This is a PDF file of an unedited manuscript that has been accepted for publication. As a service to our customers we are providing this early version of the manuscript. The manuscript will undergo copyediting, typesetting, and review of the resulting proof before it is published in its final form. Please note that during the production process errors may be discovered which could affect the content, and all legal disclaimers that apply to the journal pertain.

Raman spectroscopy predicts the link between claw keratin and bone collagen structure in a mouse model of oestrogen deficiency.

**AUTHORS:**

M. Clare Caraher<sup>1</sup>

School of Chemistry and Chemical Engineering, Queen's University Belfast, Stranmillis Road, Belfast, UK.

Antonia Sophocleous<sup>2</sup>

Rheumatology and Bone Diseases Unit, Centre for Genomic and Experimental Medicine, MRC Institute of Genetics and Molecular Medicine, Western General Hospital, University of Edinburgh, UK.

J. Renwick Beattie

J Renwick Beattie Consulting, Causeway Enterprise Agency, Ballycastle, UK.

Olive O'Driscoll

AventaMed, Rubicon Centre, Rossa Avenue, Bishopstown, Cork, Ireland.

Niamh M. Cummins

Centre for Interventions in Infection, Inflammation and Immunity, Graduate Entry Medical School, University of Limerick, Ireland.

Orlaith Brennan

Tissue Engineering Research Group, Department of Anatomy, Royal College of Surgeons in Ireland, Dublin, Ireland.

Trinity Centre for Bioengineering, Trinity College, Dublin, Ireland.

Advanced Materials and Bio-Engineering Research Centre (AMBER), RCSI & TCD, Dublin, Ireland.

Fergal J. O'Brien

Tissue Engineering Research Group, Department of Anatomy, Royal College of Surgeons in Ireland, Dublin, Ireland.

Trinity Centre for Bioengineering, Trinity College, Dublin, Ireland.

Advanced Materials and Bio-Engineering Research Centre (AMBER), RCSI & TCD, Dublin, Ireland.

Steven E. J. Bell

School of Chemistry and Chemical Engineering, Queen's University Belfast, Stranmillis Road, UK

Mark Towler

Department of Mechanical and Industrial Engineering, Ryerson University, Toronto, ON, Canada.

Stuart H. Ralston

Rheumatology and Bone Diseases Unit, Centre for Genomic and Experimental Medicine, MRC Institute of Genetics and Molecular Medicine, Western General Hospital, University of Edinburgh, UK.

Aymen I. Idris<sup>3</sup>

Rheumatology and Bone Diseases Unit, Centre for Genomic and Experimental Medicine, MRC Institute of Genetics and Molecular Medicine, Western General Hospital, University of Edinburgh, UK.

**Present Addresses:**

<sup>1</sup>ICON plc, South County Business Park, Leopardstown, Dublin, IRELAND

<sup>2</sup>Department of Life Sciences, European University Cyprus, Nicosia, Cyprus.

<sup>3</sup>Department of Oncology and Metabolism, Medical School, University of Sheffield, Beech Hill Road, Sheffield, U.K.

**RUNNING TITLE:** Raman spectroscopy predicts bone loss.

**CORRESPONDENCE TO:** Dr J. R. Beattie, J Renwick Beattie Consulting, Causeway Enterprise Agency, Ballycastle, UK. Email: rene@jrenwickbeattie.com

and

Dr A. I. Idris. Department of Oncology and Metabolism, Beech Hill Road, Sheffield, S10 2RX, UK. E-mail: aymen.idris@sheffield.ac.uk.

1. **AUTHOR EMAILS:** M. Clare Caraher (clarecaraher@gmail.com), Antonia Sophocleous (a.sophocleous@euc.ac.cy), J. Renwick Beattie (rene@jrenwickbeattie.com), Olive O'Driscoll (email:olive.odriscoll@aventamed.com), Niamh M. Cummins (email: niamh.cummins@ul.ie), Orlaith Brennan (email:OBrennan1@rcsi.ie), Fergal J. O'Brien (email: fjobrien@rcsi.ie), Steven E. J. Bell (email:s.bell@qub.ac.uk), Mark Towler (mark.r.towler@gmail.com), Stuart H. Ralston (stuart.ralston@ed.ac.uk), Aymen I. Idris (aymen.idris@sheffield.ac.uk).

## Abstract

Osteoporosis is a common disease characterised by reduced bone mass and an increased risk of fragility fractures. Low bone mineral density is known to significantly increase the risk of osteoporotic fractures, however, the majority of non-traumatic fractures occur in individuals with a bone mineral density too high to be classified as osteoporotic. Therefore, there is an urgent need to investigate aspects of bone health, other than bone mass, that can predict the risk of fracture. Here, we successfully predicted association between bone collagen and nail keratin in relation to bone loss due to oestrogen deficiency using Raman spectroscopy. Raman signal signature successfully discriminated between ovariectomised rats and their sham controls with a high degree of accuracy for the bone (sensitivity 89%, specificity 91%) and claw tissue (sensitivity 89%, specificity 82%). When tested in an independent set of claw samples the classifier gave 92% sensitivity and 85% specificity. Comparison of the spectral changes occurring in the bone tissue with the changes occurring in the keratin showed a number of common features that could be attributed to common changes in the structure of bone collagen and claw keratin. This study established that systemic oestrogen deficiency mediates parallel structural changes in both the claw (primarily keratin) and bone proteins (primarily collagen). This strengthens the hypothesis that nail keratin can act as a surrogate marker of bone protein status where systemic processes induce changes.

**KEYWORDS:** Raman Spectroscopy, bone, collagen, keratin, osteoporosis, microCT.

## Abbreviations

AUC: Area Under the Curve (for receiver operator characteristics)

BMD: Bone Mineral Density

BV/TV: Bone Volume / Total Volume (also known as bone volume density)

DXA: Dual energy X-ray Absorptiometry

LDA: Linear Discriminant Analysis

microCT: micro Computed Tomography

OVX: Ovariectomised

PCA: Principal Component Analysis

ROI: Region Of Interest

SVD: Singular Value Decomposition

## 1 Introduction

Postmenopausal osteoporosis is a common disease characterised by reduced bone mass and an increased risk of fragility fractures which increases dramatically in incidence with age [1]. The risk of osteoporosis is determined by a balance between levels of peak bone mass attained during skeletal growth and the amount of bone that is lost later on in life [2–5]. At menopause, declining oestrogen levels trigger an increase in bone remodelling with uncoupling of osteoclastic bone resorption from osteoblastic bone formation [6]. Evidence from rodent and nonhuman primate studies indicates that enhanced bone remodelling associated with deficiency in sex hormone leads to bone loss [7–10] (in humans this type of change increases risk of fragility fractures).

The majority of osteoporotic fractures occur in patients with low bone mineral density (BMD), as assessed by Dual energy X-ray Absorptiometry (DXA) [11–13]. However, there is overlap in BMD between individuals with recurrent fractures and those who have not, inferring that low BMD is not the only cause of fragile bones [10,14]. Degree of mineralization is another standard by which osteoporosis is diagnosed, however it is often

unreliable in detecting bone fragility. This is mainly due to its inability to take into account, amongst other factors [15], changes in the bone matrix protein, primarily collagen. Studies have shown that collagen in osteotropic patients exhibits a different structure to normal collagen [16,17], and have found a correlation between these structural changes in collagen and bone fracture [18,19].

Ovariectomy in large rodents is a reproducible and widely accepted model of oestrogen deficiency and reflects many changes observed in post menopausal women. For example, it leads to reduction in trabecular bone volume coupled with an increase in adipose tissues (in some rodents), phenotypes similar to those observed in aged human. Notwithstanding this the model does not account for factors such as genetic variability, life style, diet and other hormone levels that affect bone health. A key feature of this model is that the hormone deficiency is a systemic effect and as such would be expected to expose the whole body of the animal to the same risk factor. Raman spectroscopy is a sensitive and non-invasive optical technique in which the transfer of energy from light to matter gives 'fingerprint' information of a sample's chemical composition and physical state. The technique is commonly used in chemical analysis e.g. in forensic, and pharmaceutical science, however more recently it has been identified as a potential tool for evaluating bone. Using Raman spectroscopy, a comparison study of iliac crest biopsies and femoral head samples revealed that osteoporotic women with fractures had a greater carbonate/phosphate ratio in cortical bone and a higher carbonate/amide I ratio in femoral trabecular bone when compared to healthy women [20]. Other studies by Pillay *et al*, Towler *et al*. and Moran *et al*. used Raman spectroscopy to demonstrate that nails from osteoporotic patients had lower disulphide bonding compared to healthy controls [21–23]. A subsequent clinical study on 633 nail donors showed that Raman analysis of the fingernails was capable of discriminating between donors who had and who had not suffered a fragility fracture[24]. Detailed spectroscopic investigation revealed that the



structural integrity of the keratin in the nail was different between the groups, with the fracture group exhibiting a more disordered protein structure than the non-fracture group [25]. Together, these findings led to the hypothesis that changes in composition and structure of keratin (nail) in osteoporotic models may act as a surrogate marker of systemic processes that affect the structural proteins in the bone matrix (collagen).

In this study, we further tested this hypothesis by comparing the changes in claw keratin Raman spectra with the changes in the proteins, chemical composition and architectural changes due to oestrogen deficiency in rats. The hypothesis that we are testing is that systemic changes that affect bone proteins may also have a parallel impact on keratin proteins in claws.

## 2 Materials and Methods

### 2.1 Animal experiments

All animal experiments were approved by the Animal Welfare and Ethical Review Body of the University of Edinburgh (Scotland, UK) and conducted in accordance with the UK Animals (Scientific Procedures) Act 1986. Animals were housed under standard conditions of temperature ( $25 \pm 1^\circ\text{C}$ ) and relative humidity ( $60 \pm 10\%$ ) on 12 hours light/dark cycle with *ad libitum* access to standard pellet diet and tap water.

#### 2.1.1 Ovariectomy and hormone replacement

Ovariectomy or sham ovariectomy was performed in 12 weeks old Sprague-Dawley rats as previously described [26]. The experiment terminated on day 77 and bone mineral density was measured at the tibial metaphysis by micro computed tomography (microCT).

## 2.1.2 Animal study design

### 2.1.2.1 *Sprague-Dawley study design and treatments*

The Sprague-Dawley study was designed and carried out at the University of Edinburgh (Scotland, UK). The rats were randomly assigned to 1 of 3 groups: ovariectomy (OVX, n=10), sham-operated (n=10) or naïve group (n=9). All rats were sacrificed at 23 weeks of age and bone samples (right femur) were collected and stored at -20°C. Claw samples (right and left claw) were collected and stored at 4°C.

### 2.1.2.2 *Wistar study design and treatments*

The Wistar study was developed by the Royal College of Surgeons in Ireland (RCSI, Dublin, Ireland). This study details the analysis of the claw samples using Raman spectroscopy carried out at Queen's University Belfast. Under the terms of agreement bone samples were not made available. A total of 65 retired breeder Wistar rats were randomly assigned to 1 of 11 groups including those that underwent surgical intervention and age-matched controls (Table 1). After completion of surgical intervention, the claw samples (right front and hind claws and left front and hind claws – 4 claws from each specimen) were collected and stored at 4°C.

## 2.2 Micro-computed tomography

Bone architecture was assessed using Micro-computed tomography (microCT) at the University of Edinburgh (Scotland, UK). Trabecular and cortical bone parameters were analysed as previously describe by Campbell & Sophocleous [27], using a Skyscan 1172 instrument (Brucker, Belgium) set at 70kV and 142µA and at a resolution of 10µm. Images were then reconstructed by the Skyscan NRecon program and analyzed using Skyscan CTAn software. Analysis of trabecular bone at the left distal femoral metaphysis focused on a region of interest (ROI) extending 1 mm proximally from the proximal tip of the primary spongiosa. The ROI was selected adjacent to the endocortical surface using a freehand drawing tool at

five to seven different levels. Auto-interpolation between these levels produced the total ROI for all frames selected.

### 2.3 Raman spectroscopy spectra

The bones and claws were assessed using Raman spectroscopy at Queen's University Belfast (Belfast, UK). No further sample preparation was carried out.

#### 2.3.1 Sample analysis

Raman spectra were recorded in a grid pattern on bone and claw samples using a 160mW Avalon Instrument RamanStation R1 (Avalon Instruments, Belfast, UK) at excitation wavelength 785 nm with a spectral resolution  $<4\text{ cm}^{-1}$ . The samples were exposed to the laser beam for 18 seconds for the bones (cortical region) and 15 seconds for the claws with 0.25 mm distance between the laser points (laser spot size 0.05 mm). A total of 196 and 45 spectra were collected in a grid pattern on each bone and claw sample, respectively. As the protein concentration is much lower in bone than the claw, the bone measurements were completed in triplicate. The analyst was blinded to sample treatments throughout data acquisition and data processing.

#### 2.3.2 Spectral Data analysis

The acquired Raman data was processed using Matlab 2013a (Mathworks, Cambridge UK) and Labspec 6 (Horiba UK Ltd, Stanmore, UK) software. Cosmic rays were manually corrected by comparing each spectrum in the dataset with the spectra adjacent to it and identifying any sharp features ( $<3$  pixels,  $>3\times$  SNR) that occurred in only one spectrum. The data from the Sprague-Dawley animals were used to develop models for processing and analysing the Raman spectra. This included building a baseline correction model using SVD-based background correction [28,29]. All the spectra were truncated to remove peak-less regions, intensity normalised (mean intensity of spectrum), mean centred and analysed using principle component analysis (PCA) as previously described[24]. The PCA scores for

components which exhibited a significant difference between the baseline and ovariectomised groups were put into a linear discriminant analysis, along with the normalised mean centred Raman data. The resulting discriminant scores were used to calculate sensitivity, specificity and area under the curve (AUC) performance characteristics. The processing algorithms and linear discriminant analysis (LDA) model developed on the claw data acquired from the Sprague-Dawley animals was tested on the data acquired from the Wistar rat claws to determine the transferability of the model to new samples and new populations. The Wistar group was used as a validation set, with sensitivity, specificity and AUC calculated for comparison with the Sprague-Dawley animals. The same processing algorithms and LDA model was applied to the sham ovariectomy within the Sprague-Dawley set to determine its impact on collagen and keratin. To obtain partial subtraction average normalized bone and claw spectra for detailed evaluation, the average spectrum from each group was normalised to the mean intensity of the Sprague-Dawley bone or claw spectra, then partially subtracted from the sum of all the bone or claw spectra until just before any negative features appeared in the result.

#### 2.4 Sample size calculation

The sample size for the ovariectomy experiments was chosen to provide at least 80% power to detect a 1.8 standard difference (i.e. an effect size of  $\sim 1.8$ ) in different micro-CT based variables between baseline, sham-operated and OVX groups. Post hoc (retrospective) power analyses showed that the effect size achieved for BV/TV was more than double (approximately 4) and the achieved power for detecting a difference in BV/TV between sham-operated and OVX groups was 100%.

#### 2.5 Micro-CT Statistical analysis

Statistical analyses were performed using IBM (Armonk, NY) SPSS Statistics, version 19. Significant differences between groups (baseline, sham-operated and OVX) were assessed

using one-way analysis of variance (ANOVA) followed by Tukey HSD post hoc test. Power calculations were performed using G\*Power software, version 3.1.9.2 (Heinrich Heine University Düsseldorf, Germany)

### 3 Results

#### 3.1 Effects of ovariectomy on body and uterine weight

Body weight is an important determinant of bone mass and oestrogen deficiency is often associated with a significant increase in body weight [30]. As shown in Figure 1A, body weight significantly increased in Sprague-Dawley after ovariectomy. In contrast, uterine weight fell significantly after ovariectomy (data not shown), indicative of the successful removal of ovaries.

#### 3.2 Effects of ovariectomy on bone architecture

Detailed microCT analysis confirmed that ovariectomised rats had significantly lower trabecular bone volume (Figure 1B) and this was accompanied by a significant reduction in trabecular number (Figure 1C). Ovariectomy also caused a significant increase in trabecular separation (Figure 1D) and a decrease in trabecular connectivity, indicated by the increased trabecular pattern factor (Figure 1E). No significant changes were observed in trabecular thickness after ovariectomy (Figure 1F). Figure 1 (panel G) shows representative microCT images from the trabecular bone of the distal femoral metaphysis of Baseline (day zero), ovariectomised (OVX) and sham-operated Sprague-Dawley rats.

#### 3.3 Raman spectrum of bone and claw tissue compared to standards

The average Raman spectra for Sprague-Dawley bone samples were compared to the corresponding claw samples from the same model shown in Figure 2A (I & III). For comparison, hydroxyapatite mineral, collagen and keratin standard were also included

(Figure 2A II, IV & V respectively). A summary of the main peaks, their wavenumber shifts, band assignments and whether they are due to mineral, collagen or keratin are listed in Table 2. The Raman spectrum of bone is dominated by phosphate bands similar to those of the hydroxyapatite at the lower wavenumber, while at higher wavenumber the spectrum is comprised primarily of protein-like features. Collagen can be distinguished from keratin by the presence of a strong peak due to hydroxyproline (no.7) and the absence of a distinct band for tyrosine and tryptophan peak (no. 21). Despite the mineral peaks in close proximity, the hydroxyproline peaks are identifiable in the bone spectrum, while there is no evidence of the tyrosine and tryptophan peak (no. 21).

### 3.4 Evaluation of spectral differences between bone and claw treatment groups

To evaluate what impact ovariectomy is having on the structure of the bone and claw compared to their respective baseline and sham OVX treatment groups, detailed analysis of the spectra was performed. The spectra of the bone and claw were scaled to the mean intensity of the spectrum for subtraction and the subtraction spectra are presented for comparison in Figures 2B and C. The bone spectra show sham and OVX treatment groups have an elevated band at peak no. 12, which is indicative of carbonate deposition within the hydroxyapatite matrix. Comparison between baseline, sham-OVX and OVX clearly indicates OVX treatment affects both the mineral and collagen matrix phases of the bone. OVX decreased the mineral bands indicated by the peaks at lower Raman shift at peak no. 1 and 3, and increased collagen bands, indicated by stronger peaks at Raman shifts at peak no. 20 and 22-24 compared to control. In the claw Raman signatures, changes to keratin secondary structure were observed; compared to baseline, OVX reduced  $\beta$ -sheet content (peak no. 24) and resulted in an altered  $\alpha$ -helical conformation (peak shift from peak no. 22 in baseline to peak no. 23 in OVX group). Interestingly, the Raman spectral signatures for the bone and claw sham-OVX groups indicate sham OVX is subtly altering the structure of proteins in

both tissues, but at a much lower rate than the OVX. The bone sham-OVX spectra showed a reduction in the overall protein content (peak no. 13-24) compared to baseline.

### 3.5 Discrimination between healthy and osteoporotic tissue using a LDA model

In this study, using the data acquired from bone and claw spectra from an osteoporotic model, an LDA model was created in an attempt to discriminate between healthy and osteoporotic bone and claw tissue. Figure 2 (panel D) shows the Sprague-Dawley bone discriminant function (i) calculated from the LDA modelled on OVX against baseline group, and for comparison the Sprague-Dawley claw discriminant function (ii) calculated from the LDA modelled on the same treatment groups. The discriminant function highlights the variance between the treatment groups in both tissues. The prominent positive features are representative of the baseline (healthy state), whilst the prominent negative features illustrate the changes in the tissues induced by ovariectomy (osteoporotic state). The prominent positive peaks in the mineral phase of the bone discriminant function (left side of dotted line) include phosphate peaks, no. 1, 3 and 9 in the positive direction, while the carbonate peak (no.12) is a prominent negative peak. For comparison between the protein content of both tissues, the positive and negative peaks in the region right of the dotted line are highlighted. The prominent negative peaks shown in the bone collagen region of the discriminant function include C-H bone peaks (no 18 and 20) and amide I random coil peak (no. 23), and these same peaks were negative in the claw keratin discriminant function. Furthermore, the main positive peaks in the claw discriminant function, including amide I  $\alpha$ -helix and  $\beta$ -sheet peaks (no. 22 and 24 respectively), were also local maxima in the bone discriminant function. The fact that these local areas of variance, from two different tissues, were the same suggests that ovariectomy is altering the structure of collagen and keratin in a similar manner.

Figure 3A shows the Sprague-Dawley bone sample LDA results modelled on the OVX group against baseline group and projected onto the sham OVX treatment group. The LDA

classified the baseline group as significantly different compared to OVX, whilst the sham OVX group was classified as not significantly different. Moreover, the OVX group was significantly different to the baseline and sham OVX groups. To give an indication of how appropriate this model is for determining differences and similarities in bone from health and osteoporotic rat tissue using Raman spectra, the sensitivity, specificity and AUC values were calculated from the derived LDA (Table 3); this model gave 89% sensitivity, 91% specificity and an area under the curve (AUC) of 94%.

The claws showed similar levels of performance to the bone tissue. The LDA for the Sprague-Dawley rat claws (Figure 3B) classified the baseline group as significantly different compared to all of the other treatment groups, with OVX being the most significant, while OVX is significantly different from baseline and sham OVX. The Wistar rats showed no significant difference between the control and ovariectomised rats at the early stages of treatment ( $\leq 8$  weeks), but after the 12 week delay the ovariectomised rats had a significantly lower score than the control rats and also than the rats sacrificed at a younger age (Figure 3C). The Sprague-Dawley calibration set yielded a model with a sensitivity of 89% and a specificity of 82%, and AUC of 92%. The Wistar rat data used as validation of the model achieved a sensitivity of 92% and a specificity of 85%, while the AUC was 94%.

## 4 Discussion

Ageing is associated with many degenerative processes, including the weakening of bone, leading (in humans) to increased susceptibility to fracture, even in the absence of significant trauma. The rat ovariectomy model is a standard model to study postmenopausal osteoporosis in pre-clinical trials [31]. Ovariectomised rats display similar stages of osteoporosis as in humans [32], and the model allows for investigation of changes occurring against a more uniform population, using younger animals (minimising effect of different rates of ageing) in



a highly controlled environment. A key difference is that the rat models do not tend to sustain fragility fractures as a result of the deterioration in bone health. In this study, we analysed the impact of ovariectomy on bone collagen and claw keratin protein structure in ovariectomised rats using Raman spectroscopy.

Although we acknowledge that the ovariectomy model does not fully capture all of the complexities postmenopausal osteoporosis, it is widely used to explore mechanisms of bone loss and to investigate the effects of treatments for osteoporosis. In this study we have used this model to analyse the impact of ovariectomy on bone collagen and claw keratin protein structure using Raman spectroscopy. Collagen and keratin have similar structures and properties [33], and in this study we showed that these proteins have similar Raman signatures in the mineral-free region.

Formation of collagen fibres in bone involves a series of complex post-translational modifications including hydroxylation of proline and lysine, glycosylation of hydroxylysine and generation of collagen crosslinks that are often associated with bone maturation [34]. Due to the interrelationship with mineralization, it would be expected that any change to collagen structure could alter collagen fibre organization and orientation and thus the mineral to collagen ratio, all of which help regulate bone strength, flexibility and fragility [34]. Previous studies have indicated that oestrogen deficiency leads to an increased turnover of the bone collagen matrix with an imbalance in favour of resorption over formation [34]. This increased rate of collagen synthesis generates abnormalities in post-translational modifications in collagen, including over-hydroxylation of lysine residues and over-glycosylation of hydroxylysine, leading to weakened collagen fibres with fewer crosslinks that affects mineralization of the fibre [35]. Using Raman spectroscopy, we showed that ovariectomy in adult rats decreased mineral to collagen ratio compared to baseline. This result agrees with previous findings [32,36] and that shows ovariectomy increases the protein

content relative to the mineral content in the bone spectra. Raman spectra of bone in humans exhibit changes in protein content relative to mineral content across a number of bone pathologies including osteoporosis and osteogenesis imperfecta [37–39].

Keratin is a key structural protein that provides cells and tissues with resilience to withstand mechanical and chemical stress [40–43]. Previous structural Raman spectroscopy analysis revealed Keratin's resilience to be due to its highly ordered structure, mostly in the  $\alpha$ -helical conformation, with a high degree of protein folding and disulphide bond formation [44]. Thus, similar to collagen, keratin's properties most likely depend on coherent organisation and disruption of the secondary or tertiary structure of the protein would impact its ability to perform its functions. Indeed, studies by Farran *et al.* show fingernails' mechanical properties change under different conditions and this was hypothesised to occur via altered matrix flexibility caused by breakdown of disulphide bonding [45]. Evaluation of the claw Raman spectral information in this study showed substantial changes to the secondary and tertiary structure of claw keratin upon ovariectomy. The position of the amide bands for  $\alpha$ -helices is sensitive to the tertiary structure, with  $\alpha$ -helices in globular proteins giving amide I bands at a higher wavenumber position than  $\alpha$ -helices in fibrous proteins. Upon ovariectomy the Raman band corresponding to  $\alpha$ -helices is shifted to a higher position reflecting a change in tertiary structure that suggests ovariectomy is associated with a reduction in fibrous structure and an increase in globular structure. The tertiary structure of collagen is also being altered by ovariectomy in a similar manner. Compared to baseline, ovariectomy shows an increase in amide I collagen content, particularly in the globular structure as signified by a large increase in amide I peak at a higher wavenumber position indicative of random structure (peak no. 24). Similar changes (elevated intensity around  $1660\text{ cm}^{-1}$  and reduced intensity at  $1685\text{ cm}^{-1}$ ) in the amide I region from collagen of bone for ovariectomised rats has been reported by Orkoulou *et al* [46]. Keratin in claws and nails is arranged in closely fitting fibrous strands. In

this study, our data suggest that the rigid order to claw keratin fibres in ovariectomised rats was disrupted leading to a less organized keratin structure with more flexibility. Whilst these keratin changes are occurring upon ovariectomy, our results also suggest bone collagen structure is becoming less organised, which may impact on the organization and orientation of collagen fibres and thus affect mineral deposition; all of which are important in the maintenance of bone strength, toughness and fragility.

The model algorithm generated in this study was able to significantly distinguish the baseline and sham-ovariectomised groups from the ovariectomised group in bone and claw tissues. It should be noted that the animals that underwent sham-ovariectomy did show altered Raman signatures compared to both baseline and ovariectomy, but these changes are independent of those associated with the true ovariectomy as the LDA models did not classify the sham as significantly different to baseline. As control animals were not sacrificed at the later age it is not possible to identify if the changes in the sham ovariectomy are a result of natural aging compared to the baseline animals or if it could be attributed to changes induced by the body responding to the sham operation. The model illustrates that adult rats which have undergone ovariectomy have measurable differences in chemical and physical properties of the bone and claw compared to those from healthy untreated and sham rats (baseline and control models). Moreover, high sensitivity, specificity and AUC values calculated in this statistical model for the bone tissue imply that this is a suitable model for studying changes in bone collagen in relation to bone health.

In this study we also assessed whether the statistical method generated for the claws is transferable by testing the Raman derived clinical models on a second independent set of animals. The Wistar rat claw model was independent from the Sprague-Dawley claw model as they were using different species of rat and were designed and carried out in different centres. Utilising claw Raman data generated from an independent study (Wistar model)

allowed for testing of the algorithm. The algorithm did not classify the Wistar claw control and ovariectomised groups as different over shorter treatment durations; however these groups were classified as significantly different at the longer treatment duration. This agrees with the differences observed in the Sprague-Dawley claw model as the treatment duration was 11 weeks. Applying the Wistar claw data as a prediction set to the Sprague-Dawley claw data (training set) shows comparable sensitivity, specificity and AUC values indicating this model is stable when applied to new populations and allows the use of keratin as a surrogate marker of bone health. These findings indicate the model has potential for evaluating differences between healthy and osteoporotic bone and claw tissues. Although the classification model for the bone tissue was not validated within this study the performance of Raman spectroscopic methods for analysing bone tissue is well established in independent studies[47–51].

#### 4.1 Conclusions

In summary, interpretation of Raman signatures reveals that oestrogen deficiency in ovariectomised adult rats mediates changes within both bone and claw tissue. The ovariectomy-induced changes in the protein phase of both tissues are similar. Both proteins have a less ordered structure in the osteoporotic model compared to baseline, which indicate that the post-ovariectomy changes induce a greater degree of structural flexibility within collagen and keratin. It is likely that the less ordered collagen will impact on mineral deposition and thus fragility risk. Whilst, these collagen changes are occurring in the bone, our results suggest similar changes to keratin structure are happening concurrently. Thus, we provide evidence suggesting there is significant potential in using keratin as a surrogate marker for bone health deterioration.

## Funding Sources

This work was supported by Crescent Diagnostics Ltd and Intertrade Ireland (FUSION programme 2012).

## Conflict of interest

Crescent Diagnostics Ltd funded the work carried out by MCC, JRB, (OD), NMC, MT and SHR. AI and AS declare no conflict of interest.

## References

- [1] WHO, Assessment of fracture risk and its application to screening for postmenopausal osteoporosis: report of a WHO study group. Tech Rep Ser; 1994:843, Geneva, 1994. <http://apps.who.int/iris/handle/10665/39142>.
- [2] J.C. Gallagher, D. Goldgar, A. Moy, Total bone calcium in normal women: Effect of age and menopause status, J. Bone Miner. Res. 2 (2009) 491–496. doi:10.1002/jbmr.5650020605.
- [3] R. Eastell, P.D. Delmas, S.F. Hodgson, E.F. Eriksen, K.G. Mann, B.L. Riggs, Bone Formation Rate in Older Normal Women: Concurrent Assessment with Bone Histomorphometry, Calcium Kinetics, and Biochemical Markers\*, J. Clin. Endocrinol. Metab. 67 (1988) 741–748. doi:10.1210/jcem-67-4-741.
- [4] R.P. Heaney, Estrogen-calcium interactions in the postmenopause: a quantitative description, Bone Miner. 11 (1990) 67–84. doi:10.1016/0169-6009(90)90016-9.
- [5] B.E. Nordin, A.G. Need, A. Bridges, M. Horowitz, Relative contributions of years since menopause, age, and weight to vertebral density in postmenopausal women., J.

- Clin. Endocrinol. Metab. 74 (1992) 20–23. doi:10.1210/jcem.74.1.1727821.
- [6] A.J.J. Wood, B.L. Riggs, L.J. Melton, The Prevention and Treatment of Osteoporosis, N. Engl. J. Med. 327 (1992) 620–627. doi:10.1056/NEJM199208273270908.
- [7] R.P. Heaney, R.R. Recker, P.D. Saville, Menopausal changes in bone remodeling., J. Lab. Clin. Med. 92 (1978) 964–70. <http://www.ncbi.nlm.nih.gov/pubmed/739174> (accessed May 15, 2017).
- [8] R. Balena, B.C. Toolan, M. Shea, A. Markatos, E.R. Myers, S.C. Lee, E.E. Opas, J.G. Seedor, H. Klein, D. Frankenfield, et al., The effects of 2-year treatment with the aminobisphosphonate alendronate on bone metabolism, bone histomorphometry, and bone strength in ovariectomized nonhuman primates., J. Clin. Invest. 92 (1993) 2577–86. doi:10.1172/JCI116872.
- [9] V. Poli, R. Balena, E. Fattori, A. Markatos, M. Yamamoto, H. Tanaka, G. Ciliberto, G.A. Rodan, F. Costantini, Interleukin-6 deficient mice are protected from bone loss caused by estrogen depletion., EMBO J. 13 (1994) 1189–96. <http://www.ncbi.nlm.nih.gov/pubmed/8131749> (accessed May 15, 2017).
- [10] D. Marshall, O. Johnell, H. Wedel, Meta-analysis of how well measures of bone mineral density predict occurrence of osteoporotic fractures, BMJ. 312 (1996). <http://www.bmj.com/content/312/7041/1254?linkType=FULL&resid=312/7041/1254&journalCode=bmj> (accessed May 15, 2017).
- [11] J.A. Kanis, L.J. Melton, C. Christiansen, C.C. Johnston, N. Khaltsev, The Diagnosis of Osteoporosis, J. Bone Miner. Res. 9 (2009) 1137–1141. doi:10.1002/jbmr.5650090802.
- [12] C. V. Odvina, J.E. Wergedal, C.R. Libanati, E.E. Schulz, D.J. Baylink, Relationship between trabecular vertebral body density and fractures: A quantitative definition of spinal osteoporosis, Metabolism. 37 (1988) 221–228. doi:10.1016/0026-0495(88)90099-6.

- [13] R.B. Mazess, Bone density in diagnosis of osteoporosis: Thresholds and breakpoints, *Calcif. Tissue Int.* 41 (1987) 117–118. doi:10.1007/BF02563789.
- [14] P.D. Ross, R.D. Wasnich, J.M. Vogel, Detection of prefracture spinal osteoporosis using bone mineral absorptiometry, *J. Bone Miner. Res.* 3 (2009) 1–11. doi:10.1002/jbmr.5650030103.
- [15] A.L. Boskey, Bone composition: relationship to bone fragility and antiosteoporotic drug effects, *Bonekey Rep.* 2 (2013). doi:10.1038/bonekey.2013.181.
- [16] A. Bailey, S. Wotton, T. Sims, P. Thompson, Post-translational modifications in the collagen of human osteoporotic femoral head, *Biochem. Biophys. Res. Commun.* 185 (1992) 801–805. doi:10.1016/0006-291X(92)91697-O.
- [17] M. Saito, K. Fujii, S. Soshi, T. Tanaka, Reductions in degree of mineralization and enzymatic collagen cross-links and increases in glycation-induced pentosidine in the femoral neck cortex in cases of femoral neck fracture, *Osteoporos. Int.* 17 (2006) 986–995. doi:10.1007/s00198-006-0087-0.
- [18] I. Kovach, C. Agrawal, R. Richards-Kortum, X. Wang, K. Athanasiou, Laser-induced autofluorescence and fracture toughness of baboon cortical bone, in: *Proc. 43th Annu. Meet. Orthop. Soc.*, San Francisco, 1997: p. 22:37.
- [19] X. Wang, X. Shen, X. Li, C.M. Agrawal, Age-related changes in the collagen network and toughness of bone., *Bone.* 31 (2002) 1–7. doi:10.1016/S8756-3282(01)00697-4.
- [20] B.R. McCreadie, M.D. Morris, T. Chen, D. Sudhaker Rao, W.F. Finney, E. Widjaja, S.A. Goldstein, Bone tissue compositional differences in women with and without osteoporotic fracture, *Bone.* 39 (2006) 1190–1195. doi:10.1016/j.bone.2006.06.008.
- [21] I. Pillay, D. Lyons, M.J. German, N.S. Lawson, H.M. Pollock, J. Saunders, S. Chowdhury, P. Moran, M.R. Towler, The use of fingernails as a means of assessing bone health: a pilot study., *J. Womens. Health (Larchmt).* 14 (2005) 339–344.

- doi:10.1089/jwh.2005.14.339.
- [22] P. Moran, M.R. Towler, S. Chowdhury, J. Saunders, M.J. German, N.S. Lawson, H.M. Pollock, I. Pillay, D. Lyons, Preliminary work on the development of a novel detection method for osteoporosis, *J. Mater. Sci. Mater. Med.* 18 (2007) 969–974. doi:10.1007/s10856-006-0037-6.
- [23] M.R. Towler, A. Wren, N. Rushe, J. Saunders, N.M. Cummins, P.M. Jakeman, Raman spectroscopy of the human nail: A potential tool for evaluating bone health?, *J. Mater. Sci. Mater. Med.* 18 (2007) 759–763. doi:10.1007/s10856-006-0018-9.
- [24] J.R. Beattie, N.M. Cummins, C. Caraher, O.M. O'Driscoll, A.T. Bansal, R. Eastell, S.H. Ralston, M.D. Stone, G. Pearson, M.R. Towler, Raman spectroscopic analysis of fingernail clippings can help differentiate between postmenopausal women who have and have not suffered a fracture, *Clin. Med. Insights Arthritis Musculoskelet. Disord.* 9 (2016) 109–116. doi:10.4137/CMAMD.S38493.
- [25] J.R. Beattie, M.C. Caraher, N.M. Cummins, O.M. O'Driscoll, R. Eastell, S.H. Ralston, M.R. Towler, Raman spectral variation for human fingernails of postmenopausal women is dependent on fracture risk and osteoporosis status, *J. Raman Spectrosc.* (2017). doi:10.1002/jrs.5123.
- [26] A. Sophocleous, A.I. Idris, Rodent models of osteoporosis, *Bonekey Rep.* 3 (2014). doi:10.1038/bonekey.2014.109.
- [27] G.M. Campbell, A. Sophocleous, Quantitative analysis of bone and soft tissue by micro-computed tomography: applications to ex vivo and in vivo studies, *Bonekey Rep.* 3 (2014). doi:10.1038/bonekey.2014.59.
- [28] J.R. Beattie, J.J. McGarvey, Estimation of signal backgrounds on multivariate loadings improves model generation in face of complex variation in backgrounds and constituents, *J. Raman Spectrosc.* 44 (2013) 329–338. doi:10.1002/jrs.4178.



- [29] J.R. Beattie, Optimising reproducibility in low quality signals without smoothing; An alternative paradigm for signal processing, *J. Raman Spectrosc.* 42 (2011) 1419–1427. doi:10.1002/jrs.2851.
- [30] K. Mueller, S. Hsiao, Estrus- and ovariectomy-induced body weight changes: Evidence for two estrogenic mechanisms., *J. Comp. Physiol. Psychol.* 94 (1980) 1126–1134. doi:10.1037/h0077746.
- [31] P.P. Lelovas, T.T. Xanthos, S.E. Thoma, G.P. Lyritis, I.A. Dontas, The Laboratory Rat as an Animal Model for Osteoporosis Research, (n.d). <http://www.ingentaconnect.com/content/aalas/cm/2008/00000058/00000005/art00001> (accessed May 15, 2017).
- [32] T.J. Wronski, M. Cintron, A.L. Doherty, L.M. Dann, Estrogen Treatment Prevents Osteopenia and Depresses Bone Turnover in Ovariectomized Rats\*, *Endocrinology.* 123 (1988) 681–686. doi:10.1210/endo-123-2-681.
- [33] F. Colla, P. Brühlmann, R. Panizzon, B.A. Michel, [Osteopoikilosis--skin and joint manifestations], *Z. Rheumatol.* 54 (1995) 123–7. <http://www.ncbi.nlm.nih.gov/pubmed/7793159> (accessed May 15, 2017).
- [34] S. Viguet-Carrin, P. Garnero, P.D. Delmas, The role of collagen in bone strength, *Osteoporos. Int.* 17 (2006) 319–336. doi:10.1007/s00198-005-2035-9.
- [35] A.J. Bailey, S.F. Wotton, T.J. Sims, P.W. Thompson, Biochemical changes in the collagen of human osteoporotic bone matrix, *Connect. Tissue Res.* 29 (1993) 119–132. doi:10.3109/03008209309014239.
- [36] T.J. Wronski, P.L. Lowry, C.C. Walsh, L.A. Ignaszewski, Skeletal alterations in ovariectomized rats, *Calcif. Tissue Int.* 37 (1985) 324–328. doi:10.1007/BF02554882.
- [37] G.S. Mandair, M.D. Morris, Contributions of Raman spectroscopy to the understanding of bone strength, *Bonekey Rep.* 4 (2015).

- p>doi:10.1038/bonekey.2014.115.
- [38] B.R. Mccreadie, M.D. Morris, T.-C. Chen, D.S. Rao, W.F. Finney, E. Widjaja, S.A. Goldstein, Bone tissue compositional differences in women with and without osteoporotic fracture, (2006). doi:10.1016/j.bone.2006.06.008.
- [39] K. Buckley, J.G. Kerns, J. Vinton, P.D. Gikas, C. Smith, A.W. Parker, P. Matousek, A.E. Goodship, Towards the in vivo prediction of fragility fractures with Raman spectroscopy, *J. Raman Spectrosc.* 46 (2015) 610–618. doi:10.1002/jrs.4706.
- [40] E. Fuchs, D.W. Cleveland, A structural scaffolding of intermediate filaments in health and disease, *Science* (80-. ). 279 (1998) 514–519. doi:10.1126/science.279.5350.514.
- [41] K. Seltmann, A.W. Fritsch, J.A. Käs, T.M. Magin, Keratins significantly contribute to cell stiffness and impact invasive behavior., *Proc. Natl. Acad. Sci. U. S. A.* 110 (2013) 18507–12. doi:10.1073/pnas.1310493110.
- [42] L. Ramms, G. Fabris, R. Windoffer, N. Schwarz, R. Springer, C. Zhou, J. Lazar, S. Stiefel, N. Hersch, U. Schnakenberg, T.M. Magin, R.E. Leube, R. Merkel, B. Hoffmann, Keratins as the main component for the mechanical integrity of keratinocytes., *Proc. Natl. Acad. Sci. U. S. A.* 110 (2013) 18513–8. doi:10.1073/pnas.1313491110.
- [43] L. Farren, S. Shayler, A.R. Ennos, The fracture properties and mechanical design of human fingernails, *J. Exp. Biol.* 207 (2004). <http://jeb.biologists.org/content/207/5/735.short> (accessed May 15, 2017).
- [44] M. Gniadecka, O.F. Nielsen, D.H. Christensen, H.C. Wulf, Structure of Water, Proteins, and Lipids in Intact Human Skin, Hair, and Nail, *J. Invest. Dermatol.* 110 (1998) 393–398. doi:10.1046/j.1523-1747.1998.00146.x.
- [45] L. Farran, A.R. Ennos, S.J. Eichhorn, The effect of humidity on the fracture properties of human fingernails, *J. Exp. Biol.* 211 (2008).

- <http://jeb.biologists.org/content/211/23/3677.short> (accessed May 15, 2017).
- [46] M.G. Orkoulas, M.Z. Vardaki, C.G. Kontoyannis, Study of bone matrix changes induced by osteoporosis in rat tibia using Raman spectroscopy, *Vib. Spectrosc.* 63 (2012) 404–408. doi:10.1016/j.vibspec.2012.09.016.
- [47] E.R. Draper, M.D. Morris, N.P. Camacho, P. Matousek, M. Towrie, A.W. Parker, A.E. Goodship, Novel Assessment of Bone Using Time-Resolved Transcutaneous Raman Spectroscopy, *J. Bone Miner. Res.* 20 (2005) 1968–1972. doi:10.1359/JBMR.050710.
- [48] M.D. Morris, G.S. Mandair, Raman Assessment of Bone Quality, *Clin. Orthop. Relat. Res.* 469 (2011) 2160–2169. doi:10.1007/s11999-010-1692-y.
- [49] J. Shen, L. Fan, J. Yang, A.G. Shen, J.M. Hu, A longitudinal Raman microspectroscopic study of osteoporosis induced by spinal cord injury, *Osteoporos. Int.* 21 (2010) 81–87. doi:10.1007/s00198-009-0949-3.
- [50] J.-L.H. Demers, F.W.L. Esmonde-White, K.A. Esmonde-White, M.D. Morris, B.W. Pogue, Next-generation Raman tomography instrument for non-invasive in vivo bone imaging, *Biomed. Opt. Express.* 6 (2015) 793. doi:10.1364/BOE.6.000793.
- [51] G.S. Mandair, F.W.L. Esmonde-White, M.P. Akhter, A.M. Swift, J. Kreider, S.A. Goldstein, R.R. Recker, M.D. Morris, Potential of Raman spectroscopy for evaluation of bone quality in osteoporosis patients: results of a prospective study, in: N. Kollias, B. Choi, H. Zeng, R.S. Malek, B.J. Wong, J.F.R. Ilgner, K.W. Gregory, G.J. Tearney, L. Marcu, H. Hirschberg, S.J. Madsen, A. Mandelis, A. Mahadevan-Jansen, E.D. Jansen (Eds.), *International Society for Optics and Photonics*, 2010: p. 754846. doi:10.1117/12.842515.
- [52] E. Widjaja, G.H. Lim, A. An, A novel method for human gender classification using Raman spectroscopy of fingernail clippings, *Analyst.* 133 (2008) 493. doi:10.1039/b712389b.

- [53] M. Garland, J.S. Morris, M.J. Stampfer, G.A. Colditz, V.L. Spate, C.K. Baskett, B. Rosner, F.E. Speizer, W.C. Willett, D.J. Hunter, Prospective Study of Toenail Selenium Levels and Cancer Among Women, *JNCI J. Natl. Cancer Inst.* 87 (1995) 497–505. doi:10.1093/jnci/87.7.497.
- [54] J.T. Pelton, L.. McLean, Spectroscopic Methods for Analysis of Protein Secondary Structure, *Anal. Biochem.* 277 (2000) 167–176. doi:10.1006/ABIO.1999.4320.

## Figure legends

**Figure 1.** Effects of ovariectomy model on Sprague-Dawley rats. (A) Body weight (g) in ovariectomised and sham-operated Sprague-Dawley rats. (B-F) MicroCT analysis of trabecular bone at the distal femoral metaphysis (B, trabecular bone volume, BV/TV, %; C, trabecular number, Tb.N,  $\mu\text{m}$ ; D, trabecular separation, Tb.Sp,  $\mu\text{m}$ ; E, trabecular pattern factor, Tb.Pf,  $1/\mu\text{m}$ ; F, trabecular thickness, Tb.Th,  $\mu\text{m}$ ;). The values shown are mean  $\pm$  sem. \* $p < 0.05$  vs. Sham by one-way analysis of variance (ANOVA). (G) Representative microCT images from the trabecular bone of the distal femoral metaphysis of Baseline (day zero), ovariectomised (OVX) and sham-operated Sprague-Dawley rats.

**Figure 2.** Effect of ovariectomy model on The Raman signatures of bone and claw tissues. (A) Average normalised Raman spectra of Sprague-Dawley bone (i) and claw (iii) samples. The average spectra for the bone and claw models are compared to hydroxyapatite (ii), collagen (iv) and keratin (v). (B-C) Subtraction spectra for average (i) ovariectomy and (ii) sham ovariectomy minus baseline from bone (B) and claw (C) samples. Selected Raman bands are labelled against table 2 with the corresponding wavelength in brackets. (D) The discriminant function for Sprague-Dawley bone (i) and claw (ii) samples as determined by the linear discriminant analysis (LDA) modeled on the respective ovariectomised (OVX) group against baseline group and projected onto the other treatment groups. The mineral peaks ( $350\text{-}1100\text{cm}^{-1}$ ) are labeled in the bone spectra including peak number and wavenumber. While the corresponding protein peaks ( $1100\text{-}1800\text{cm}^{-1}$ ) in the bone collagen and claw keratin are indicated including peak number and wavenumber.

**Figure 3.** Mean scores for ovariectomy discriminant models (built on OVX vs baseline, applied to sham). A) Sprague-Dawley bone tissue B) Sprague-Dawley claw tissue and C) model derived from Sprague Dawley claw tissue applied to Wistar rat claw tissue. The Wistar animals were split into those culled within 8 and 12 or more weeks of study start, with

the longer growth time being used as the validation set for the model. Error bars represent 95% confidence interval. Significance between Control and each treatment group (indicated by \* and solid lines), and between OVX and each treatment group (indicated by \* and dotted lines) was measured. \*\*  $p < 0.01$ , \*\*\* $p < 0.001$ .

ACCEPTED MANUSCRIPT

## Tables

4.2 Table 1. Wistar study design.

Group	Surgical intervention	Duration (weeks)	(n)
1	None	0	4
2	None	2	6
3	OVX	2	6
4	None	4	6
5	OVX	4	6
6	None	8	6
7	OVX	8	6
8	None	12	6
9	OVX	12	6
10	None	20	7
11	OVX	20	6

*The table lists the number of different groups according to duration and the number of samples in each group. Ovariectomy (OVX).*

Table 2. Bone and Claw Raman spectroscopy Band Assignments.

Peak No.	Raman Shift (cm <sup>-1</sup> )	Assignment	Keratin/Collagen/Mineral	References
1	430	$\text{PO}_4^{3-} \nu_2 \text{ AS}$	Mineral	[48]
2	510	Disulfide, $\nu$ (S-S)	Keratin	[23]
3	580-590	$\text{PO}_4^{3-} \nu_4 \text{ AS}$	Mineral	[48]
4	644	Cysteine, $\nu$ (CS)	Keratin	[22]
5	830	Tyrosine, $\delta$ (CCH) <sub>OP</sub>	Collagen/Keratin	[52]
6	850	Tyrosine/O-P-O, $\delta$ (CCH) ring breathing	Collagen/Keratin/Mineral	[52]
7	856	Hydroxyproline	Collagen	[48]
8	936	$\alpha$ -helix, $\nu$ (CC)	Collagen/Keratin	[52]
9	960	$\text{PO}_4^{3-} \nu_1$	Mineral	[48]



10	1004	Phenylalanine	Collagen/Keratin	[52]
11	1032	Phenylalanine	Collagen/Keratin	[52]
12	1070	$\text{CO}_4^{3-} (\nu)$	Mineral	[53]
13	1078	Carbon backbone, $\nu (\text{CC})_{\text{RC}}$	Collagen/Keratin	[52]
14	1126	Carbon backbone, $\nu (\text{CC})_{\text{TC}}$	Collagen/Keratin	[52]
15	1206	Tyrosine and Phenylalanine, $\nu (\text{C}-\text{C}_6\text{H}_5)$	Collagen/Keratin	[52]
16	1240	$\beta$ -sheet, Amide III	Collagen/Keratin	[48]
17	1256	Random, Amide III	Collagen/Keratin	[52]
18	1305	$\alpha$ -helix, Amide III	Collagen/Keratin	[48]
19	1420	C-H bonding, $\delta (\text{CH}_3)$ deformation	Collagen/Keratin	[52]
20	1450	C-H bonding, $\delta (\text{CH}_2)$ scissoring	Collagen/Keratin	[52]
21	1614	Tyrosine and Tryptophan, C=C stretching	Keratin	[52]

<b>22</b>	1642-44	$\alpha$ -helix, $\nu$ (CO) amide I	Collagen/Keratin	[54]
<b>23</b>	1652-56	Random, $\nu$ (CO) amide I	Collagen/Keratin	[54]
<b>24</b>	1668-75	$\beta$ -sheet, $\nu$ (CO) amide I	Collagen/Keratin	

---

The main peaks present in the bone and claw spectra are listed in numerical order including their wavenumbers, band assignments, whether they are keratin, collagen or mineral bands and band assignment references. Asymmetric stretch (AS), out of plane ( $\gamma$ ), in plane ( $\delta$ ) random conformation (RC), trans conformation (TC) and stretch ( $\nu$ ).

	OVX vs Control	(n <sub>control</sub> )	(n <sub>OVX</sub> )	Sensitivity (%)	Specificity (%)	AUC (%)
Bone	Sprague-Dawley	9	11	89	91	94
	(12 weeks)					
Claw	Sprague-Dawley	9	11	89	82	92
	(12 weeks)					
	calibration model					
	Wistar	13	12	92	85	94
	(≥12 weeks)					
	validation model					

Table 3. Linear discriminant analysis (LDA) was modelled on ovariectomised (OVX) group against control group and projected onto the other treatment groups in the bone samples.

The sensitivity, specificity and AUC (area under the curve) values are shown.

Figure 1.

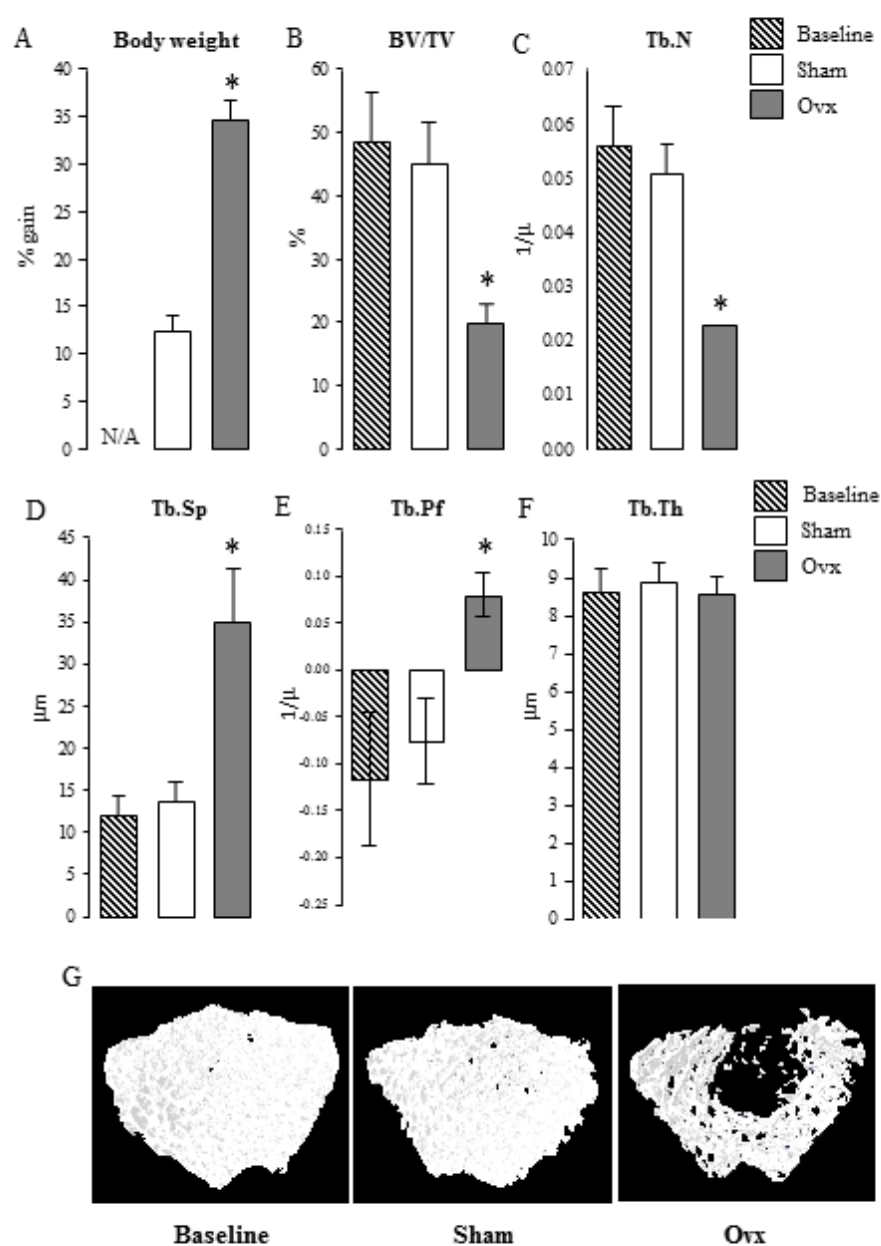


Figure 2.

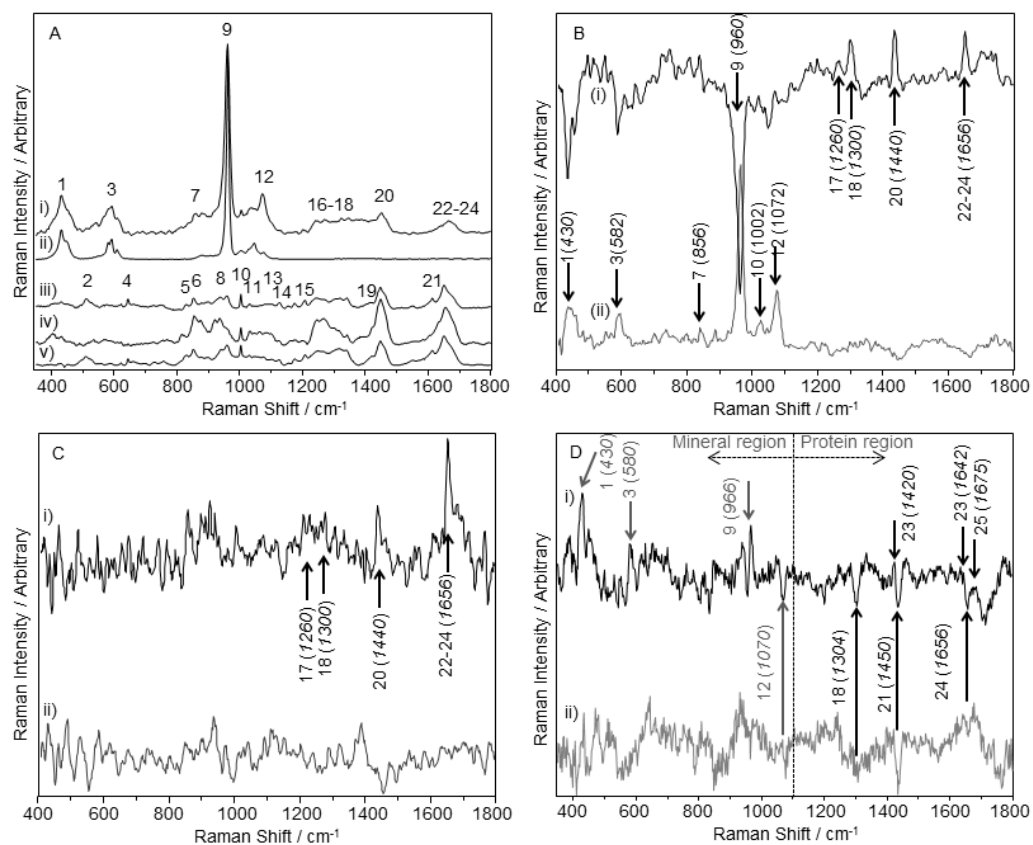
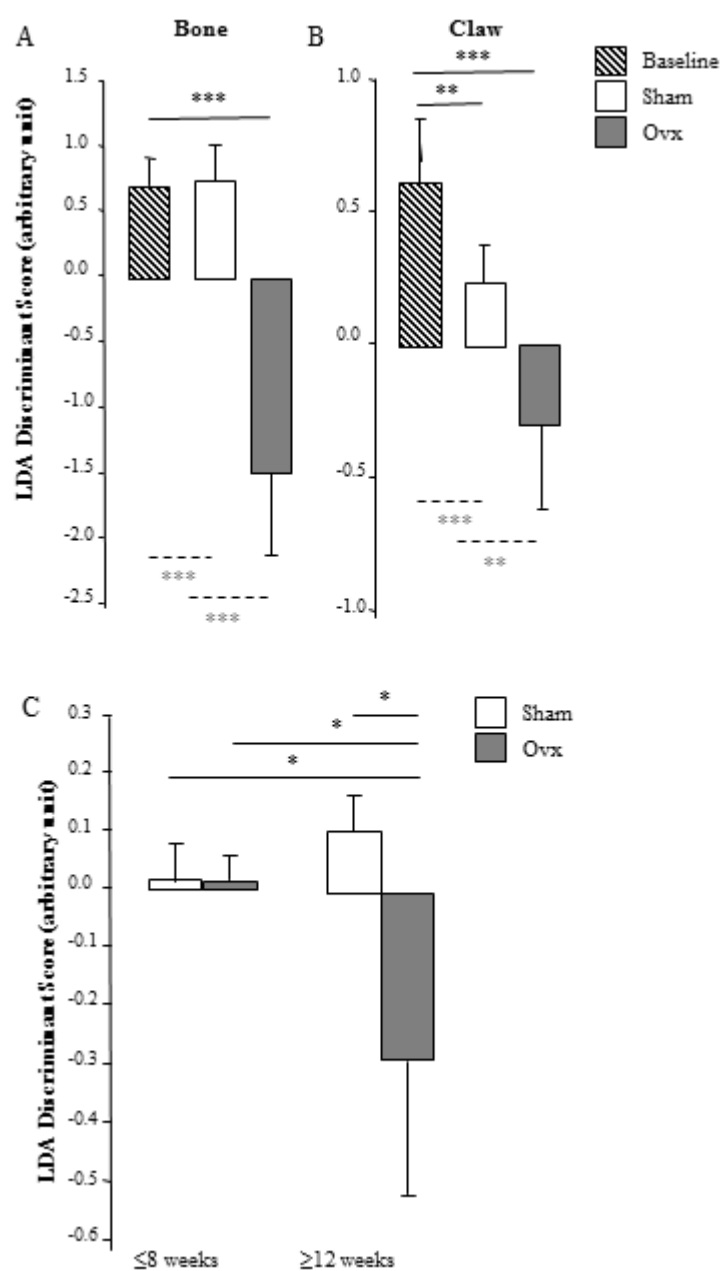
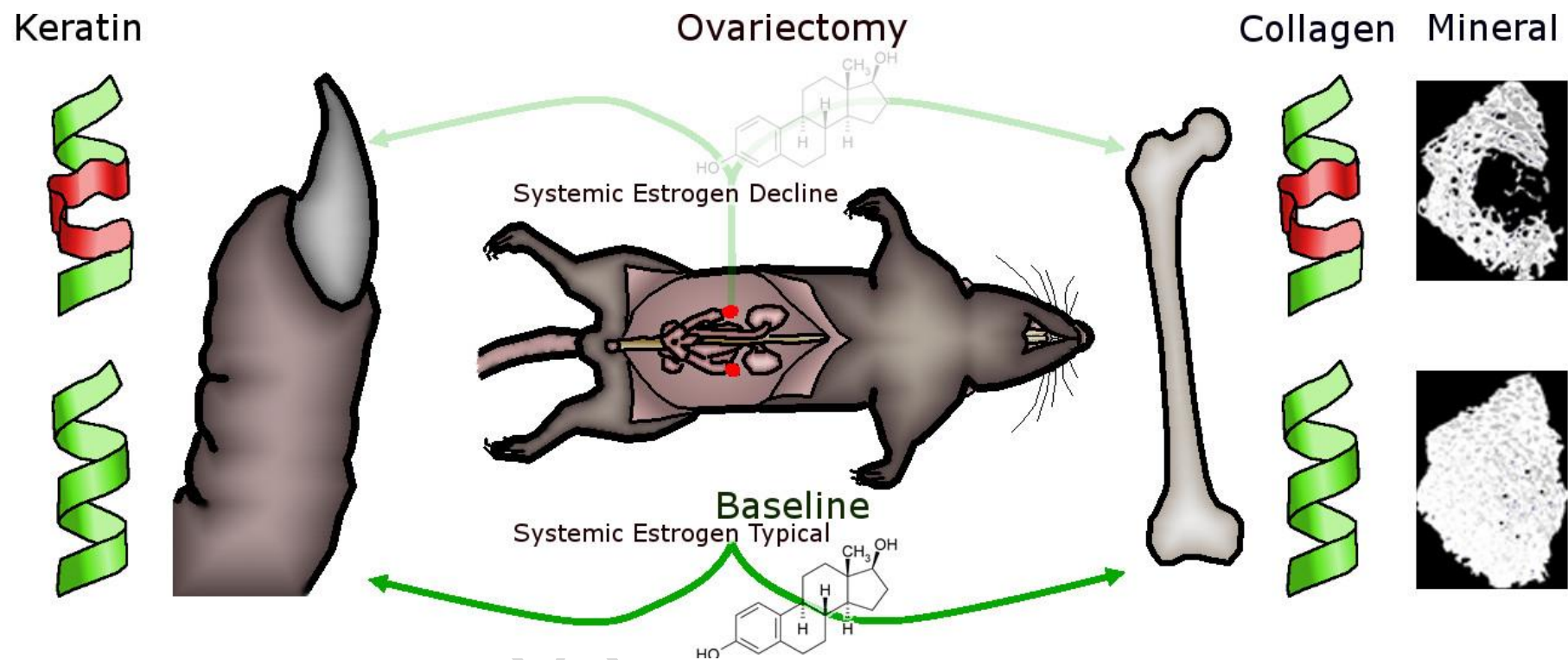


Figure 3.





Graphical abstract

### Highlights

- Ovariectomy, which reduces systemic estrogen concentrations, influences remote tissues in a rat model
- Mineral decline observed in rat bone in both mineral and protein matrices
- Protein matrix of both bone and claw showed decrease in ordered structure and increase in disordered structure
- Propose hypothesis that systemic processes can affect structural proteins in both the bone (primarily collagen) and claw (primarily keratin)